Supporting Online Material

Materials and Methods

Ribosome purification and crystallization. Ribosomes lacking protein S1 were purified from *E. coli* strain MRE600 using sucrose gradient centrifugation, as described (*S1*). Ribosomes were crystallized at 18°C using microbatch 96-well plates and buffers containing 4-5% 2-methyl-2,4-pentanediol (MPD), 3.9-4.4% PEG 8000, 3.8 mM $MgCl_2$, 380 mM NH_4Cl, 5.5 mM putrescine, 5 mM spermidine, 10 mM Tris plus 20 mM MES, pH=6.5-7.0, and 0.25 mM EDTA. For complexes containing mRNA and ASL^{Met}_f, 5 μM mRNA of sequence 5'p-AUGUUU-3' and 10 μM of ASL^{Met}_f (nucleotides 27-43 of $tRNA^{Met}_f$) (Dharmacon) were included in the crystallization trials. For complexes containing mRNA and ASL^{Phe}, 5 μM mRNA of sequence U_6 and 10 μM of ASL^{Phe} (nts 27-43 of $tRNA^{Phe}$) were included.

Structure determination. Ribosome crystals were stabilized with crystallization buffer containing 7% MPD, 7% PEG 8000 and 12% PEG 400, pH=4.8, to allow cryocooling of the crystals to liquid nitrogen temperatures. Diffraction data were measured from crystals cooled to 100 K using 0.1-0.3° oscillations at beamline 24ID-E at the Advanced Photon Source or at the SIBYLS (12.3.1) beamline at the Advanced Light Source, each of which is equipped with an ADSC Q315 area detector. Data were reduced using Denzo/Scalepack (*S2*) and Truncate (*S3*), yielding the statistics shown in Table S1.

Molecular replacement and structure refinement. The two copies of the 70S ribosome in the crystallographic asymmetric unit were located using the program Phaser (*S4*) and atomic-resolution structures of the *E. coli* ribosome (*S1, S5*). The resulting structural models were then refined using rounds of manual rebuilding (*S6*) and torsional dynamics (*S7*). Additional stereochemical restraints were used to maintain stable rounds of refinement during early cycles of modeling, as described (*S1*). The final positional and TLS refinement of the structures was carried out using Phenix (*S8*). Electron density maps were generated using the programs Pirate (*S9*) and CNS (*S7*).

Least-squares superpositions. Comparisons to atomic-resolution structures of the ribosome, and to structural models of the intact ribosome refined against cryo-EM density maps, were carried out by least-squares superposition in the program O (*S6*), using ribose C1' positions in nucleotides. Superpositions to identify the relative position of the small and large subunits in the ribosome used the large subunit as the frame of reference (*S10*). Superpositions of the small subunits with each other utilized conserved 16S rRNA nucleotides in the body, platform and head domains of the small subunit (*S11*). Comparisons to cryo-EM reconstructions of the *E. coli* or *T. thermophilus* 70S ribosome were made after first refining the 3.4 Å structures presented here, plus tRNAs and mRNA taken from the *T. thermophilus* 70S ribosome (*S12, S13*), as a series of rigid bodies against structure factors (amplitudes and phases) derived from a series of cryoEM reconstructions (*S13*-*S17*). The rastering of the cryo-EM reconstruction in

(*16*) was reduced ~3.2%, and that in (*S14*) by ~1.9% to minimize the refinement residual.

Discussions of representative ratcheted states rely on structures of post-initiation complexes (*S5, S14*) and post-termination complexes (*S18-S20*) for state R_0; mRNA decoding and pre- or post-translocation states (*S12, S15, S17*) for state R_1; and ribosomes with tRNAs in hybrid A/P and/or P/E states (*S13, S17*) for state R_F. The distinction between states R_0 and R_1 has not been noted before, and is most pronounced with respect to the positioning of the body of the 30S subunit (Table S3). Rotation angles presented in Table S3 correspond to roughly 0.5 Å per degree for bridges B2a and 1.2 Å per degree at bridge B7a. The rotation angles for the body domain do not include opening and closing of the domain around the 30S A site, a separate and nearly orthogonal degree of freedom described in (*S21*) in the context of mRNA decoding. Angles and distances given for the rotation of the head domain were calculated from 30S subunit structures taken from 70S ribosomes in different states (*S12-S14, S17, S18*) and superimposed by means of their platform domains. A rotation of 0° is defined as centering the head domain over the 30S P site.

Figure preparation. Figures were made using the program Pymol (*S22*).

Conformation of Bridge B4 in State R_0

Protein S15, which forms an essential bridge (bridge B4) between the platform of the 30S subunit and rRNA helix H34 in the 50S subunit (*S23*), is shifted half way to its position in the fully rotated state R_F (*S10, S13, S17*) (Figure 3C). To accommodate the shift in the position of protein S15, helix H34 in 23S rRNA of the large subunit flexes to maintain essentially identical contacts with the small subunit (Fig. S2). A larger degree of bending likely occurs when the ribosome is in a fully rotated conformation (*S13*). Maintenance of bridge B4 may be important to ensure that the two subunits stay associated during the rotation motions (*S10, S23*).

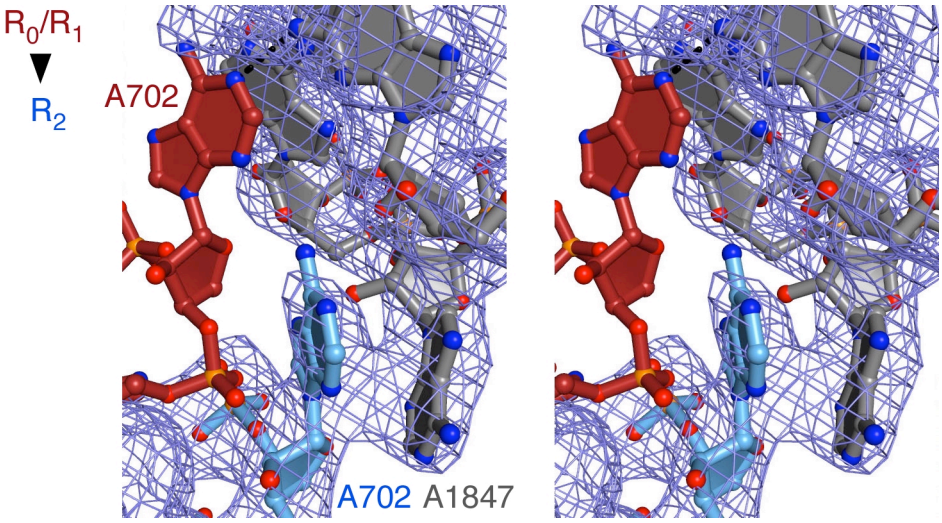

Figure S1. Stereo view of the electron density map near bridge B7a. The ribosome in state R_2 (blue, grey) is shown compared to states R_0 (*5, 18-20*) or R_1 (*12*) (red) superimposed using the 50S subunit as reference (*10*). Electron density, derived from Pirate (*9*), is contoured at 0.8 standard deviations from the mean.

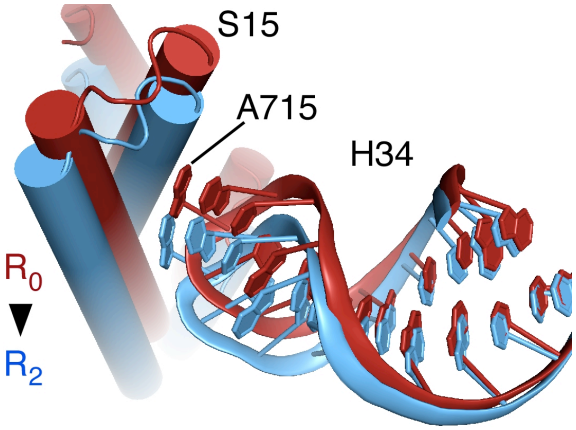

Figure S2. Bridge B4 between the ribosomal subunits in the apo-70S ribosome in state R_2. Bridge B4 in state R_2 (light blue) compared to that in state R_0 (*5*) (red). Nucleotide A715 in 23S rRNA helix H34 is marked.

Movie S1. This animation shows the changes in the 30S subunit that are proposed to occur as the ribosome ratchets from state R_0 to R_F. It shows the ratcheting motion from the perspective of the 50S subunit and is color-coded as in Figure 2. The proposed sites of tRNA binding are also shown in cartoon form for each ratcheted state conformation in the animation.

Movie S2. This animation shows the changes in the 30S subunit that are proposed to occur as the ribosome ratchets from state R_0 to R_F, emphasizing changes in the position of the 30S head domain.

Table S1. X-ray crystallographic statistics

Crystal	apo-70S	ASL^{Met}_f	2 x ASL^{Phe}
Space group	$P2_12_12_1$	$P2_12_12_1$	$P2_12_12_1$
a (Å)	211.9	210.7	211.0
b (Å)	434.9	435.1	433.1
c (Å)	622.9	628.7	624.5
Resolution (Å)	40 – 3.2	76 – 3.8	73 – 3.7
(high-resolution shell)*	(3.52-3.45)	(4.28-4.09)	(4.27-4.07)
R_{merge}	17.1 (73.2)	11.1 (38.1)	7.8 (32.2)
I / σ (I)†	6.9 (2.0)	6.9 (2.1)	7.9 (2.0)
Completeness (%)	96.2 (94.5)	78.8 (67.4)	75.9 (64.0)
Measurement redundancy	4.7 (3.6)	2.2 (1.7)	2.2 (1.4)
Unique reflections	905,214 (44,284)	438,691 (37,300)	452,913 (37,902)
No. crystals used	1	2	1

*Data beyond the high-resolution shell in parenthesis was used for refinement and map calculation, and extend to an I / σ (I) of about 1.

†All statistics not in parentheses include data over the whole reported resolution range.

Table S2. X-ray structure refinement

Crystal	Apo-70S	ASL^{Met}_{f}	2 x ASL^{Phe}
Resolution (Å)	40 – 3.2	76 – 3.8	73 – 3.7
No. Reflections	904,039	438,242	452,724
R_{free} Set	18,191	8,838	9,160
R/R_{free} (%)	19.5/25.2	20.7/25.3	22.7/26.8
No. Atoms	284,560	285,465	286,195
TLS domains*	38	40	42
R.m.s. deviations			
Bond lengths (Å)	0.006	0.007	0.006
Bond angles (°)	1.45	1.55	1.52
Mean ADP values ($Å^2$)†			
State R_2 70S	63.5	105.4	123.3
State R_0 70S	132.6	146.3	203.5

*Refinement in phenix (*S8*) with multiple TLS groups.

†Atomic displacement parameter values are reported as isotropic B-factors.

Table S3. Rotations of 30S domains during subunit ratcheting

State	Body	Platform	Central bridges	Head*
R_0	0° (±1°)	0° (±1°)	0° (±2°)	0° (±1°)
R_1	3°	1°	2°	0°
R_2	6°	5°	3°	11°
R_F	8°	8°	6°	5°, 14°‡

*Rotations of the head domain are about an axis nearly orthogonal from the ratcheting axis (Fig. 1, Fig. 4E) (*S1, S10, S24*). Structures that served as reference states for measuring head rotations were PDB entries 3D5A and 3D5B for state R_0 (*S18*), PDB entries 2J02 and 2J03 for state R_1(*S12*), the present structures for state R_2, and the cryo-EM reconstruction in (*S13*).

‡The large rotation of the head domain in R_F is estimated from cryo-EM reconstructions of the yeast ribosome (*S10, S24*), and is similar to a structure of an *E. coli* apo-70S ribosome in state R_0 (*S1*). The smaller rotation is derived from the cryo-EM reconstruction presented in (*S13*).

References

S1. B. S. Schuwirth *et al.*, *Science* **310**, 827-34 (2005).

S2. Z. Otwinowski, W. Minor, in *Methods in Enzymology* C. W. Carter Jr., R. M. Sweet, Eds. (Academic Press, New York, 1997), vol. 276, pp. 307-326.

S3. Collaborative Computing Project No. 4, *Acta Crystallographica* **D50**, 760-763 (1994).

S4. A. J. McCoy, R. W. Grosse-Kunstleve, L. C. Storoni, R. J. Read, *Acta Crystallogr D Biol Crystallogr* **61**, 458-64 (2005).

S5. V. Berk, W. Zhang, R. D. Pai, J. H. Cate, *Proc Natl Acad Sci U S A* **103**, 15830-4 (2006).

S6. T. A. Jones, J. Y. Zou, S. W. Cowan, Kjeldgaard, *Acta Crystallogr. A* **47**, 110-9 (1991).

S7. A. T. Brünger *et al.*, *Acta Crystallogr. D Biol. Crystallogr.* **54**, 905-21 (1998).

S8. P. D. Adams *et al.*, *Acta Crystallogr D Biol Crystallogr* **58**, 1948-54 (2002).

S9. K. Cowtan, *Acta Crystallogr D Biol Crystallogr* **56 Pt 12**, 1612-21 (2000).

S10. J. Frank, H. Gao, J. Sengupta, N. Gao, D. J. Taylor, *Proc Natl Acad Sci U S A* **104**, 19671-8 (2007).

S11. J. J. Cannone *et al.*, *BMC Bioinformatics* **3**, 2 (2002).

S12. M. Selmer *et al.*, *Science* **313**, 1935-42 (2006).

S13. S. R. Connell *et al.*, *Mol Cell* **25**, 751-64 (2007).

S14. I. S. Gabashvili *et al.*, *Cell* **100**, 537-49 (2000).

S15. E. Villa *et al.*, *Proc Natl Acad Sci U S A* **106**, 1063-8 (2009).

S16. G. S. Allen, A. Zavialov, R. Gursky, M. Ehrenberg, J. Frank, *Cell* **121**, 703-12 (2005).

17. X. Agirrezabala *et al.*, *Mol Cell* **32**, 190-7 (2008).

18. M. Laurberg *et al.*, *Nature* **454**, 852-7 (2008).

19. A. Korostelev *et al.*, *Proc Natl Acad Sci U S A* **105**, 19684-9 (2008).

20. A. Weixlbaumer *et al.*, *Science* **322**, 953-6 (2008).

21. J. M. Ogle, F. V. Murphy, M. J. Tarry, V. Ramakrishnan, *Cell* **111**, 721-32 (2002).

22. W. L. Delano, *The PyMOL User's Manual* (Delano Scientific, San Carlos, CA, USA., 2002).

23. U. Maivali, J. Remme, *RNA* **10**, 600-4 (2004).

24. C. M. Spahn *et al.*, *EMBO J* **23**, 1008-19 (2004).